Ceramics International 49 (2023) 2115–2120

Contents lists available at ScienceDirect

Ceramics International

journal homepage: www.elsevier.com/locate/ceramint

Realization of room temperature exchange bias effect in Co/NiO bilayer via all-solid-state Li-ion redox capacitor

Zeeshan Mustafa [a,b], Nawishta Jabeen [c], Najam Ul Hassan [d,*], Mohsan Jelani [e], Adnan Qaiser Muhammad [f], Fatima Sehar [g], Nadeem Nasir [h], Asim Idrees [h,**], Ahmad Hussain [i], Majeed A. Bajaber [j]

[a] Lahore Garrison University, Lahore, 52400, Punjab, Pakistan
[b] Ningbo Institute of Materials Technology and Engineering, CAS, Ningbo, China
[c] Department of Physics, Fatima Jinnah Women University, Rawalpindi, 46000, Pakistan
[d] Department of Physics, Division of Science and Technology, University of Education, Lahore, 54000, Pakistan
[e] Department of Physics, University of Kotli Azad Jammu and Kashmir, Kotli, 11100, Pakistan
[f] College of Physics & Optoelectronic Engineering, Shenzhen University, Shenzhen, 518060, China
[g] Lahore College for Women University, Lahore, Pakistan
[h] Department of Applied Sciences, National Textile University, Faisalabad, 37610, Pakistan
[i] Department of Physics, The University of Lahore, Sargodha Campus, Sargodha, 40100, Pakistan
[j] Department of Chemistry, Faculty of Science, King Khalid University, Abha, 61413, Saudi Arabia

ARTICLE INFO

Keywords:
Exchange bias
Co/NiO heterostructures
Solid-state Li-Ion capacitor
Spintronic devices

ABSTRACT

The electric field-controlled exchange bias effect has drawn considerable attention of researchers as it shows great application scope in the development of modern low power consuming spintronic devices. In this research work, we have realized a reversible controlled exchange bias effect in Co/NiO heterostructures by utilizing all-solid-state Li-ion redox capacitors having antiferromagnetic electrodes, at room temperature. The nonvolatile and reversible control of exchange bias is obtained at room temperature, resulting from controlled intercalation and deintercalation of Li-ion in antiferromagnetic NiO via galvanostatic charge and discharge process. The ion migration-controlled exchange bias mechanism in Co/NiO heterostructures is studied by using various structural, electrochemical and magnetic characterizations. This work designs an approach to control the exchange bias phenomena in all-solid state magnetoionics at room temperature, which has potential importance in establishing modern spintronic devices such as magnetic random-access memories.

1. Introduction

The pinning of magnetic spins at the interface of a ferromagnetic (FM) and antiferromagnetic material (AF) is known as exchange bias (EB). The basic reason for EB is the exchange coupling of spins at the FM–AF interface and it results in shifting the magnetic hysteresis loop. The phenomenon of EB shows potential applications in many modern spintronic devices such as; magnetic random access memory and the magnetic read head. In these devices, pinned FM layer is very important and acts as a reference layer [1–3]. Nowadays, electric field control EB has been gaining great interest from researchers due to its potential applications in tunable low-power EB systems [4].

It is reported that EB can be effectively tailored in different ways such as; when a thin FM layer of an EB system is interfaced with a piezoelectric material, resulting in the transfer of strain from piezoelectric material to the FM layer and altering the value of EB field (HEB) [5–8]. Another way to tune the EB effect is the modulation of the density of charge careers at the surface of metallic AF substances, in which applied voltage exerts a force on the exchange spring, resulting in a positive or negative change in HEB [9]. The sign of HEB depends on the sign of bias voltage. Recently, it is also reported that EB can be controlled by spin-orbit coupling induced by an electric current, leading to horizontally positive or negative shifting of EB hysteresis at low temperatures. The positive/negative shift depends upon the polarity of the current

* Corresponding author.
** Corresponding author.
E-mail addresses: najam.hassan@ue.edu.pk (N.U. Hassan), asimidrees@ntu.edu.pk (A. Idrees).

https://doi.org/10.1016/j.ceramint.2022.09.177
Received 6 June 2022; Received in revised form 30 August 2022; Accepted 13 September 2022
Available online 22 September 2022

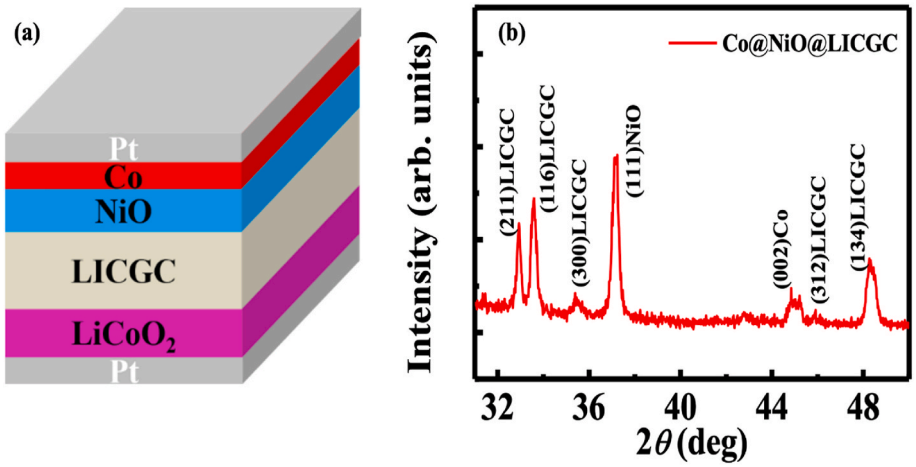

Fig. 1. (a) Schematic illustration of the all solid-state Li-ion redox capacitor. (b) XRD Pattern of as-deposited Co/NiO bilayer.

pulse [10].

An effective way to tune the magnetic properties of materials is electrically driven ion migrations, leading to effective results [11–17]. The utilization of oxygen ion has been proved to be a potential way for ionic controlled migration, where electric field-coefficient β reaches more than 5000 fJ which is very high as compared to previously used techniques. The electric field-coefficient β corresponds to interfacial magneto-crystalline anisotropy energy per voltage per unit length [13, 18]. It is also reported that reversible toggling of state from AF to FM can be obtained in SrCoO2.5 using oxygen ion migration at low values of voltage [17]. The oxygen ion migration technique has been also employed to tune the EB phenomena in Ref. [19] Si/SiO2/Pt/Co/NiO/Pt [20] and Pt/Co/NiHfO2 compounds. Owing to rich chemistry, Li-ion migration effective technique for magnetic properties as it promotes better diffusion at room temperature [16]. Li-ion migration facilitates to control of the various magneto-responsive effects such as; magnetic cycling, magnetic anisotropy, on-off magnetism and remnant magnetization of bulk magnetic materials [21–24].

In this research work, we have controlled the EB phenomena at room temperature in Co/NiO heterostructures by utilizing all-solid-state Li-ion redox capacitors using electric field-driven controlled Li-ion migration. When Li-ion transports into the AF NiO electrode, leads to producing spin disorder due to a conversion reaction between oxygen ions. A systematic investigation to control the Li-ion migration-controlled EB phenomena has been made using structural, magnetic and electrochemical characterizations. As a result, an EB control has been realized at room temperature using all-solid state magnetoinics.

2. Experiment

(i) Sample Preparation:

The proposed all-solid-state Li-ion redox capacitor has been fabricated as follows; the Li-ion conducting glass-ceramic (LICGC) with general composition Li2O–Al2O3–SiO2–P2O5-GeO2, is used as substrate and also as solid-state electrolyte. The pulsed laser deposition (PLD) technique is used to deposit a 250 nm thick layer of LiCoO2 as cathode material on one side of the polished LICGC to supply the Li-ion. The temperature of the substrate was kept at 873 K under an oxygen pressure of 20 Pa. A Pt layer of thickness 70 nm is deposited over LiCoO2

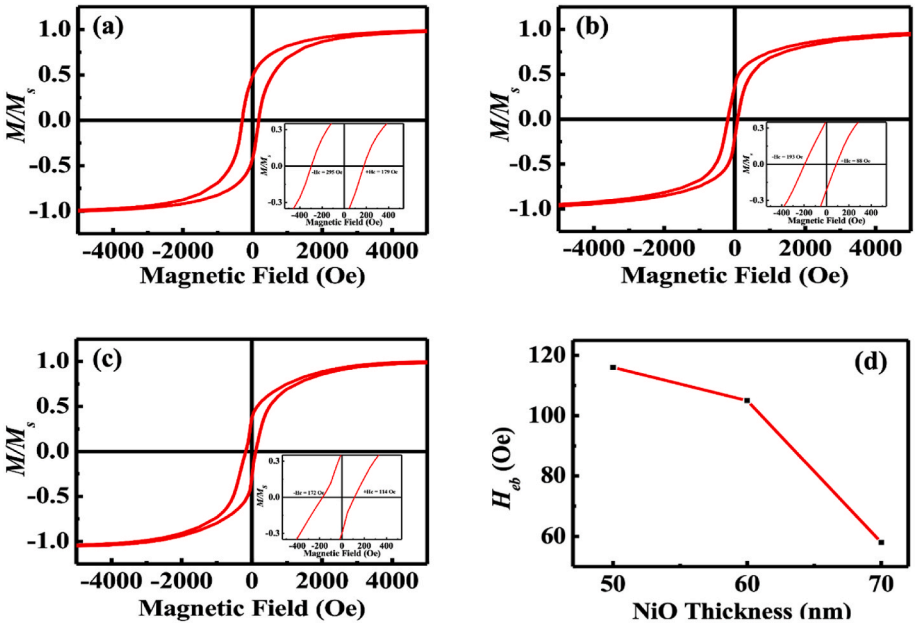

Fig. 2. (a) Normalized *MH* loop measured for (a) Co(20 nm)/NiO(50 nm), (b) Co(20 nm)/NiO(60 nm) and (c) Co(20 nm)/NiO(70 nm) bilayer deposited on LICGC. The inset of every figures shows central part of MH loop at room temperature (d) H_{EB} versus thickness of NiO curve.

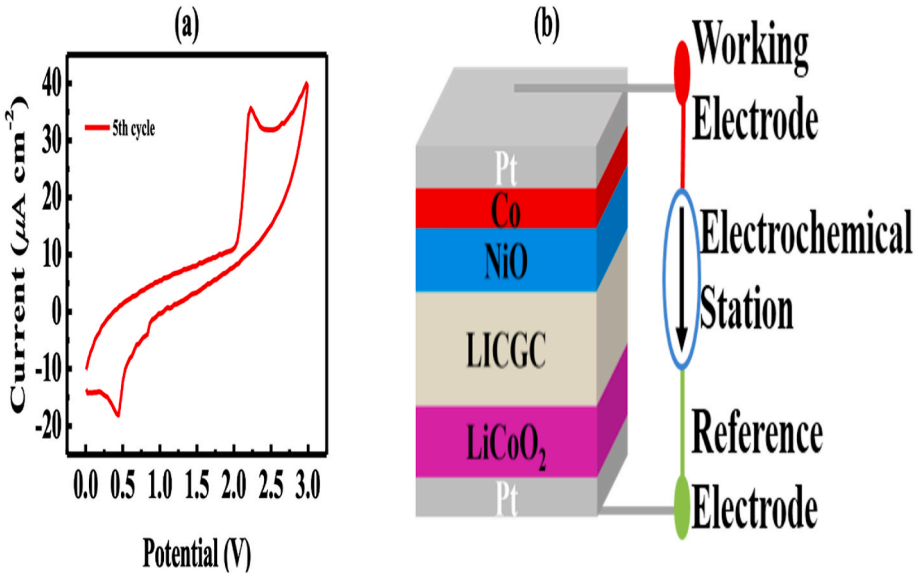

Fig. 3. (a) CV curves of the Pt/Co/NiO/LICGC/LCO/Pt hetrostructures. (b) The inset Schematic illustration of GCD at application of potential difference.

to get Pt electrode using magnetron sputtering technique. In magnetron sputtering 0.6 Pa Ar pressure with 20 W power is used. The function of this Pt electrode is as a current collector. Before growing NiO films on the other side, the diamond polishing liquid is used to remove the silver paste used as glue to clamp the LICGC on the sample holder to deposit LiCoO2. PLD technique is used to deposit the 50–70 nm thick NiO films under 30 Pa oxygen pressure and 873 K deposition temperature. A 20 nm Co film is deposited over NiO using magnetron sputtering at Ar pressure of 1.2 Pa and 20 W power and the substrate temperature is maintained at 393 K. The Pt electrode is deposited over the Co layer which acts as a current collector.

(ii) Structure and Magnetic Measurements:

X-ray diffraction (XRD) is employed to identify the structural phases of the prepared sample. XRD is carried out using Bruker D-8 DISCOVER diffractometer using Cu Kα radiation of a wavelength of 1.5406 A0 at a scan rate of 0.020 per second. A superconducting quantum interference device (SQUID) is used to perform the magnetic hysteresis (MH) loop. The investigation of change in stretching and bending modes of the charged and discharged is done In Situ. Raman spectroscopy using the Renishaw Invia Reflex Raman spectrometer. A Talos F200x is used to perform the HRTEM of prepared samples. The samples for HRTEM are prepared by using the Auriga Carl Zeiss dual beam-focused ion beam.

(iii) Electrochemical Characterization:

The galvanostatic charge-discharge (GCD) cycles and cyclic voltammetry (CV) measurements in all-solid-state Li-ion redox capacitor are carried out by using a Zahner Zennium electrochemical work station. A potential difference of 0–2.3 V at current densities of 2–6 μA cm-2 is used to perform GCD measurements while CV measurements are carried out at a potential difference of −0 to 3 V at a scan rate of 100 m Vs-1 [25,26]. Moreover, NiO acts as a working electrode while LiCoO2 is used as a counter and reference electrode as well.

3. Results & discussions

(i) Exchange Bias Effect in Co/NiO Heterostructures

Fig. 1(a) shows the schematic illustration of deposited heterostructures while the XRD pattern of as-deposited Pt/Co/NiO/LICGC/LCO/Pt thin films is shown in Fig. 1(b), indicating the crystalline nature of the structure. The indexed peaks at 33.1, 33.84, 35.3, 46.12 and 48.37° correspond to reflections of LIGCC solid electrolyte while the peaks at 37.14 and 48.88° correspond to NiO (111) and Co (002), respectively [21,27,28].

The normalized MH loops at room temperature are measured to investigate the EB in Co/NiO heterostructures. In order to measure the MH loops, the thickness of Co was fixed at 20 nm but NiO was taken as 50, 60 and 70 nm, as shown in Fig. 2 (a), (b) and (c). The obtained curves show typical ferromagnetic behaviour for all thicknesses. It can be seen that the MH curve clearly shifts to the negative field, which is evidence of exchange bias phenomena [29] The most important reasons for the formation of the thin layer EB system are the thickness of the AF layer and the interfacial roughness of FM and AF layers [30,31]. The EB arises from the uncompensated spins resulting from the combined optimal roughness of FM and AF thin films at their interfaces [31,32].

The HEB dependence on NiO thickness is shown in Fig. 2(d). A decrease in HEB is observed with an increase in the thickness of NiO. The HEB of 116, 105 and 58 Oe were observed at 50, 60 and 70 nm, and the enlarged central part of the MH loops are shown in insets. The change in HEB with respect to the thickness of NiO can be understood by the domain-state model in a better way. This model predicts that the domain-state spin changes on changing the thickness of AF material. It also relates the realization of HEB with defects in AF material. Actually, the thickness of AF plays a crucial role in getting HEB. The previously reported research also shows that the thickness of AF up to a certain limit cause's increase in defects, which leads to the domain formation in AF [33].

(ii) Control of EB by Li-ion transport

The CV curves of Pt/Co/NiO/LICGC/LCO/Pt drawn in the voltage range of 0–3 V, are shown in Fig. 3 (a). The two Pt electrodes at the top and bottom of the structure are used to apply the bias voltage, as shown in Fig. 3(b). The oxidation and reduction processes are confirmed from the CV measurements, confirming the intercalation and deintercalation of Li-ion into AF NiO [34]. The oxidative and reductive peaks are obtained at 2.2 V and 0.45 V, respectively. The oxidation and reduction processes are the signature of an electrochemical reaction taking place between an electropositive Li-ion and electronegative oxygen via conversion reactions. The intercalation and deintercalation of Li-ion at different electrode potentials are responsible for the redox reactions

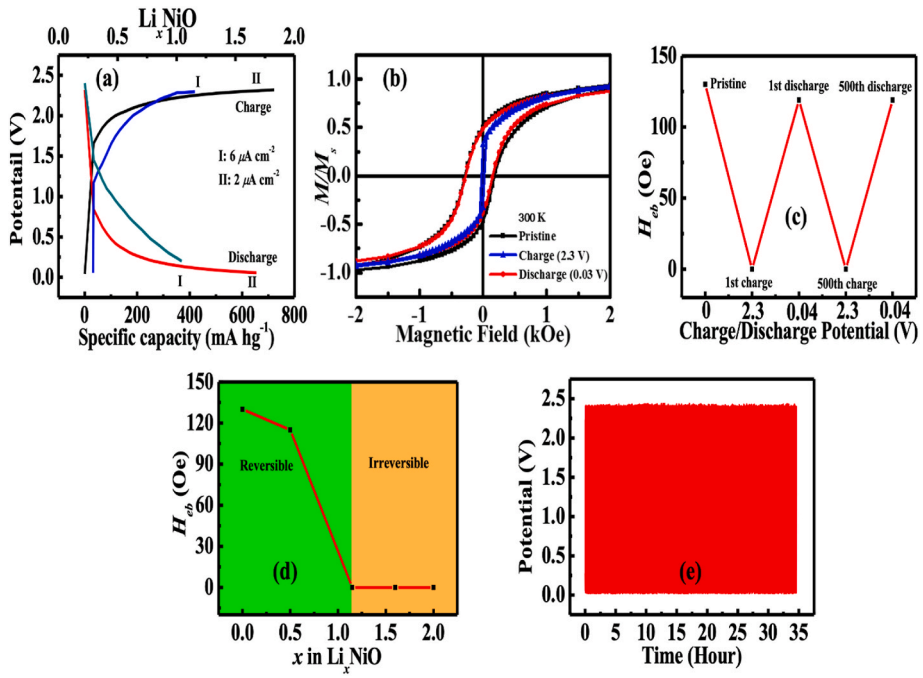

Fig. 4. (a) GCD measurements at current densities of 6 and 2 μA *Cm*-2. (b) The inset Schematic illustration of GCD at application of potential difference. (c) Room temperature normalized MH loop using SQUID VSM at pristine, charged, and discharged states. (d) *H*EB as a function of galvanostatic charge-discharge voltage from pristine state. *H*EB versus different values of x in LixNiO. (e) Cycling stability of Pt/Co/NiO/LICGC/LCO/Pt structure.

only, as no Li-ion can be stored or redox reactions occur in Ni due to its inability to react with Li-ion [35].

In order to check the stability of all-solid-state capacitors, the GCD is obtained in the voltage range of 0–2.3 V at current densities of 6 and 2 μA cm−2, as shown in Fig. 4(a) [36,37]. The high value of specific capacity is observed at 2 μA cm−2. The device exhibits a strong GCD stability for 500 cycles at a current density of 2 μA cm−2 [Fig. 4(c)]. Only 3% irreversible capacity loss is observed after the first charge and discharge cycle and is stable up to 500 charge-discharge cycles, indicating that the material is highly stable. The nonlinear behavior in the charge-discharge profile is the signature of the occurrence of electrochemical redox reactions during Li-ion intercalation and deintercalation. Faraday's law of electrolysis (Equation (1)) can be used to determine the quantity of the Li-ions (x) per formula unit of NiO under constant current electrolysis.

$$X = \frac{CM_{wt}}{F} \tag{1}$$

Here C is specific charge capacity, M_{wt} is the molecular weight of NiO and F is Faraday's constant. It is clear from Fig. 4(a) that the value of x depends upon the GCD potential difference and not on constant current density.

The pristine state exhibits a H_{EB} of 116 Oe at room temperature, as shown in the normalized MH loop. As potential difference reaches a critical value, the H_{EB} decreases. Which is due to the fact that the number of Li-ion concentrations is very small at low values of applied potential difference. The concentration of Li-ion in the NiO electrode increases when increasing the potential difference from the critical value. The observed normalized MH loop shows zero H_{EB} for $x = 1.15$ concentration of Li-ion, resulting from the distortion in the interface [Fig. 4(b)]. The H_{EB} returns to 96 Oe as when the sample is discharged in the potential difference of 30 mV. Therefore, the H_{EB} onset temperature observed to be at room temperature after first discharge shows that the Co layer is exchanged coupled with NiO. The irreversible capacity loss which results in irreversible structural changes in the material may be responsible for the decrease in observed H_{EB}. Furthermore, the reversible control of H_{EB} is observed up to the 500th GCD cycle after the first

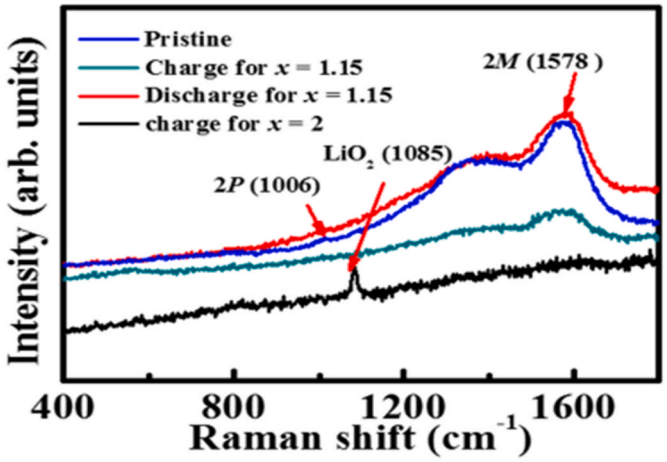

Fig. 5. Raman spectra for pristine charged to $x = 1.15$ and $x = 2$ in the range of 400–2000 cm^{-1}.

charge-discharge process, as shown in Fig. 4 (c). H_{EB} as a function of x in Li_xNiO is also measured with x ranging from 0 to 2, as shown in Fig. 4 (d). A gradual decrease in H_{EB} is observed when x is increased from 0 to 0.5, but H_{EB} decreases and reaches zero with a further increase of x from 0.5 to 1.15. No H_{EB} is observed when x increases from 1.15 to 2. For $x \leq 1.15$, the control of H_{EB} is irreversible but for $x \geq 1.15$ it is irreversible. This irreversible behaviour of H_{EB} shown by GCD for $x \geq 1.15$ can be attributed to a permanent change in the magnetic ordering of the Co/NiO structure. It is very important to understand the irreversibility of H_{EB} for $x \geq 1.15$, therefore the Li-ion inserted samples with values of $x =$ 0 (Pristine), 1.15 and 2 are investigated by advanced structural studies such as Raman spectroscopy and Tunneling electron microscopy (TEM) in next sections. Moreover, the stability of the material is checked for 1000 cycles but also can be run for more than that. The materials exhibit good stable behaviour, as shown in Fig. 4(e).

Raman spectroscopy is a vital tool to confirm the crystal structure,

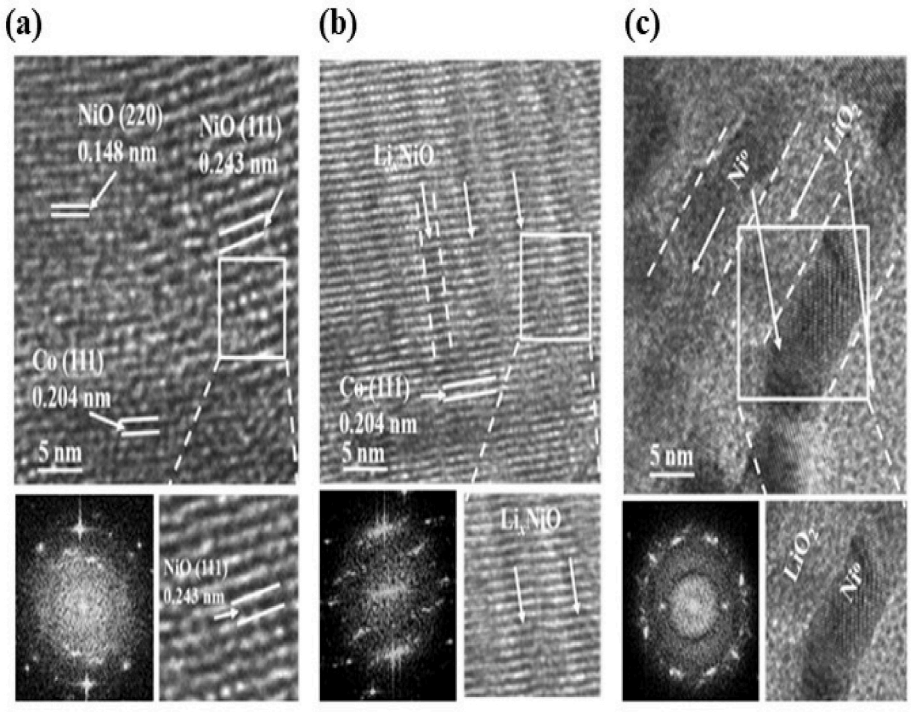

Fig. 6. TEM images of Co/NiO hetrostructures in (a) pristine state, (b) charged to $x = 0.5$, and (c) charged to $x = 1.2$. In addition, the enlarged region of Co_3O_4 and its corresponding FFT are shown for (a), (b), and (c).

defects and vacancies of the fabricated samples. Fig. 5 unrevealed the Raman spectra of pristine NiO. For the pristine NiO case, the Raman feature observed at 1006 cm^{-1} and the strong band at 1578 cm^{-1} are linked to 2P (LO + TO) and 2 M scattering resulting from Brillouin zone edge magnons of NiO, linked with super-exchange symmetry of Ni^{2+}-O^{2-}-Ni^{2+}. It is also noticed, that 2 M peak intensity varies and is broadened in the doped sample, therefore, the doping effect created more Ni^{3+0} cations, nickel vacancies, and non-stoichiometric features compared with pristine NiO [38]. During charging, the Raman intensity is suppressed for 2 M mode which represents the characteristics symmetry of NiO. The reverse trend is seen in Raman spectra during discharging for $x = 0.5$, however, the peak shifting is negligible. Clearly, after the insertion of Li-ion, the Li-ions tend to diffuse in octahedral interstitial sites compared with tetrahedral interstitial sites, due to higher interstitial positions owned by the octahedral site than the tetrahedral site [27]. Previous results showed that the singular Li atom is more compatible at the octahedral site compared with the tetrahedral site due to Fermi energy [39]. Therefore, during charging, the preferred occupancy of Li ions at octahedral Ni^{2+} sites create strain in Ni–O stretching band. Raman peaks reverted to their original values after discharge. Again for charging $x = 2$, the Raman peak linked with 2 M mode shows a broad spectrum which indicates the larger strain, additionally peak located at 1085 cm^{-1} corresponds to LiO_2.

Furthermore, TEM investigations have been carried out for pristine and charged materials to make a qualitative understanding of strain in the lattice of NiO after the lithiation process. The interface of Co/NiO for pristine, charged for x = 1.15 and x = 2 is shown in Fig. 6(a), (b) and (c), respectively. The average d spacing values calculated by HRTEM for Co and NiO are 0.204 and 0.148 nm, respectively. The given d spacing values from HRTEM measurements correspond to the (111) plane of Co and (111) plane of NiO. It can be seen from the magnified image of HRTEM that NiO exhibits an ordered structure in a pristine state and the spiral structure of NiO is confirmed by the corresponding fast Fourier transform (FFT) image. After charging to x = 1.15, the d spacing is increased and the structure changes to a partially rock-salt crystalline structure which confirms expansion in the volume of the lithiated region. This volume expansion agrees well with Raman spectroscopy discussed in the previous section. For x = 2, the NiO structure transforms to amorphous LiO2 and Ni–O as a whole and the formation of LiO2 is confirmed by the halo-diffused FFT. This is consistent with Raman spectroscopy of LixNiO when charged to x = 2 (see Fig. 6).

4. Conclusion

The EB has been successfully realized in Co/NiO heterostructures via all-solid-state Li-ion redox capacitors at room temperature. The nonvolatile and reversible Ion migration-controlled EB is achieved by the induction of a reversible spin disorder in the AF NiO by intercalation and deintercalation of Li-ion. The controlled mechanism of EB in Co/NiO heterostructures via Li-ion intercalation and deintercalation is explained on the basis of detailed structural, magnetic and electrochemical properties such as XRD, Raman, TEM, CV and GCD. This research work provides a way to tune the properties of AF oxide materials in nonvolatile and reversible manners. Additionally, it is a different technique to modulate the AF properties via Li-ion solid-state capacitor as compared to Li + chemical reactions such as alloying, insertion and conversion reactions.

Declaration of competing interest

The authors declare that they have no known competing financial interests or personal relationships that could have appeared to influence the work reported in this paper.

Acknowledgements

Majed A. Bajaber express appreciation to the Deanship of Scientific Research at King Khalid University Saudi Arabia through research groups program under grant number R.G.P. 2/167/43.

References

[1] M. Takagishi, K. Koi, M. Yoshikawa, T. Funayama, H. Iwasaki, M. Sahashi, The applicability of CPP-GMR heads for magnetic recording, IEEE Trans. Magn. 38 (2002) 2277–2282.

[2] P. Grünberg, Exchange anisotropy, interlayer exchange coupling and GMR in research and application, Sensor Actuator Phys. 91 (2001) 153–160.

[3] R.L. Comstock, Review modern magnetic materials in data storage, J. Mater. Sci. Mater. Electron. 13 (2002) 509–523.

[4] M.B. Jungfleisch, W. Zhang, A. Hoffmann, Perspectives of antiferromagnetic spintronics, Phys. Lett. 382 (2018) 865–871.

[5] P. Li, C. Zhou, C. Cao, W. Wang, C. Jiang, Electric-field control of non-volatile 180° switching of the unidirectional anisotropy field in a multiferroic heterostructure, Phys. Chem. Chem. Phys. 20 (2018) 25854–25860.

[6] S. Wu, J. Miao, X. Xu, W. Yan, R. Reeve, X. Zhang, Y. Jiang, Strain-mediated electric-field control of exchange bias in a Co90Fe10/BiFeO3/SrRuO3/PMN-PT heterostructure, Sci. Rep. 5 (2015) 1–5.

[7] M. Liu, J. Lou, S. Li, N.X. Sun, E-Field control of exchange bias and deterministic magnetization switching in AFM/FM/FE multiferroic heterostructures, Adv. Funct. Mater. 21 (2011) 2593–2598.

[8] S. Polisetty, W. Echtenkamp, K. Jones, X. He, S. Sahoo, C. Binek, Piezoelectric tuning of exchange bias in a BaTiO 3/Co/CoO heterostructure, Phys. Rev. B 82 (2010), 134419.

[9] Y. Wang, X. Zhou, C. Song, Y. Yan, S. Zhou, G. Wang, C. Chen, F. Zeng, F. Pan, Electrical control of the exchange spring in antiferromagnetic metals, Adv. Mater. 27 (2015) 3196–3201.

[10] P.-H. Lin, B.-Y. Yang, M.-H. Tsai, P.-C. Chen, K.-F. Huang, H.-H. Lin, C.-H. Lai, Manipulating exchange bias by spin–orbit torque, Nat. Mater. 18 (2019) 335–341.

[11] L.H. Diez, Y. Liu, D.A. Gilbert, M. Belmeguenai, J. Vogel, S. Pizzini, E. Martinez, A. Lamperti, J. Mohammedi, A. Laborieux, Nonvolatile ionic modification of the Dzyaloshinskii-Moriya interaction, Phys. Rev. Appl. 12 (2019), 034005.

[12] R. Mishra, D. Kumar, H. Yang, Oxygen-migration-based spintronic device emulating a biological synapse, Phys. Rev. Appl. 11 (2019), 054065.

[13] B. Dieny, M. Chshiev, Perpendicular magnetic anisotropy at transition metal/oxide interfaces and applications, Rev. Mod. Phys. 89 (2017), 025008.

[14] C. Bi, Y. Liu, T. Newhouse-Illige, M. Xu, M. Rosales, J. Freeland, O. Mryasov, S. Zhang, S. Te Velthuis, W. Wang, Reversible control of Co magnetism by voltage-induced oxidation, Phys. Rev. Lett. 113 (2014), 267202.

[15] U. Bauer, L. Yao, A.J. Tan, P. Agrawal, S. Emori, H.L. Tuller, S. Van Dijken, G. S. Beach, Magneto-ionic control of interfacial magnetism, Nat. Mater. 14 (2015) 174–181.

[16] A. Molinari, H. Hahn, R. Kruk, Voltage-control of magnetism in all-solid-state and solid/liquid magnetoelectric composites, Adv. Mater. 31 (2019), 1806662.

[17] N. Lu, P. Zhang, Q. Zhang, R. Qiao, Q. He, H.-B. Li, Y. Wang, J. Guo, D. Zhang, Z. Duan, Electric-field control of tri-state phase transformation with a selective dual-ion switch, Nature 546 (2017) 124–128.

[18] B. Cui, C. Song, F. Li, X. Zhong, Z. Wang, P. Werner, Y. Gu, H. Wu, M. Saleem, S. Parkin, Electric-field control of oxygen vacancies and magnetic phase transition in a cobaltite/manganite bilayer, Phys. Rev. Appl. 8 (2017), 044007.

[19] L. Wei, Z. Hu, G. Du, Y. Yuan, J. Wang, H. Tu, B. You, S. Zhou, J. Qu, H. Liu, Full electric control of exchange bias at room temperature by resistive switching, Adv. Mater. 30 (2018), 1801885.

[20] X. Zhou, Y. Yan, M. Jiang, B. Cui, F. Pan, C. Song, Role of oxygen ion migration in the electrical control of magnetism in Pt/Co/Ni/HfO2 films, J. Phys. Chem. C 120 (2016) 1633–1639.

[21] D. Pravarthana, B. Wang, Z. Mustafa, S. Agarwal, K. Pei, H. Yang, R.-W. Li, Reversible control of magnetic anisotropy and magnetization in amorphous Co 40 Fe 40 B 20 thin films via all-solid-state Li-ion redox capacitor, Phys. Rev. Appl. 12 (2019), 054065.

[22] X. Zhu, J. Zhou, L. Chen, S. Guo, G. Liu, R.W. Li, W.D. Lu, In situ nanoscale electric field control of magnetism by nanoionics, Adv. Mater. 28 (2016) 7658–7665.

[23] S. Dasgupta, B. Das, Q. Li, D. Wang, T.T. Baby, S. Indris, M. Knapp, H. Ehrenberg, K. Fink, R. Kruk, Toward on-and-off magnetism: reversible electrochemistry to control magnetic phase transitions in spinel ferrites, Adv. Funct. Mater. 26 (2016) 7507–7515.

[24] S. Dasgupta, B. Das, M. Knapp, R.A. Brand, H. Ehrenberg, R. Kruk, H. Hahn, Intercalation-driven reversible control of magnetism in bulk ferromagnets, Adv. Mater. 26 (2014) 4639–4644.

[25] Y. Liu, D. Wang, C. Zhang, Y. Zhao, P. Ma, W. Dong, Y. Huang, T. Liu, Compressible and lightweight MXene/carbon nanofiber aerogel with "layer-strut" bracing microscopic architecture for efficient energy storage, Adv. Fiber Mater. 4 (2022) 820–831.

[26] D. Li, X. Long, Y. Wu, H. Hou, X. Wang, J. Ren, L. Zhang, D. Yang, Y. Xia, Hierarchically porous and defective carbon fiber cathode for efficient Zn-air batteries and microbial fuel cells, Adv. Fiber Mater. 4 (2022) 795–806.

[27] Z. Mustafa, D. Pravarthana, B. Wang, H. Yang, R.-W. Li, Manipulation of exchange bias effect via all-solid-state Li-ion redox capacitor with antiferromagnetic electrode, Phys. Rev. Appl. 14 (2020), 014062.

[28] H. Gebretinsae, M. Tsegay, Z. Nuru, Biosynthesis of nickel oxide (NiO) nanoparticles from cactus plant extract, Mater. Today Proc. 36 (2021) 566–570.

[29] C. Vaz, E. Altman, V. Henrich, Exchange bias and interface electronic structure in Ni/Co 3 O 4 (011), Phys. Rev. B 81 (2010), 104428.

[30] E. Demirci, M. Öztürk, R. Topkaya, S. Kazan, N. Akdoğan, M. Obaida, K. Westerholt, Thickness and temperature dependence of exchange bias in Co/CoO bilayers, J. Supercond. Nov. Magnetism 25 (2012) 2591–2595.

[31] J. Nogués, I.K. Schuller, Exchange bias, J. Magn. Magn Mater. 192 (1999) 203–232.

[32] A.M. Choukh, Effect of interface on exchange coupling in NiFe/FeMn system, IEEE Trans. Magn. 33 (1997) 3676–3678.

[33] U. Nowak, K.-D. Usadel, J. Keller, P. Miltényi, B. Beschoten, G. Güntherodt, Domain state model for exchange bias, I. Theor. Phys. Rev. B 66 (2002), 014430.

[34] Z.-W. Fu, Y. Wang, Y. Zhang, Q.-Z. Qin, Electrochemical reaction of nanocrystalline Co3O4 thin film with lithium, Solid State Ionics 170 (2004) 105–109.

[35] V. Pralong, J.-B. Leriche, B. Beaudoin, E. Naudin, M. Morcrette, J.-M. Tarascon, Electrochemical study of nanometer Co3O4, Co, CoSb3 and Sb thin films toward lithium, Solid State Ionics 166 (2004) 295–305.

[36] X. Li, W. Chen, Q. Qian, H. Huang, Y. Chen, Z. Wang, Q. Chen, J. Yang, J. Li, Y. W. Mai, Electrospinning-based strategies for battery materials, Adv. Energy Mater. 11 (2021), 2000845.

[37] Y. Chen, M. Xu, Y. Huang, A. Manthiram, Creating a rechargeable world, Chem 8 (2022) 312–318.

[38] A. Abdallah, M. Noun, R. Awad, Dielectric, impedance and conductivity properties of pristine and (Gd, Ru)-dual doped NiO nanoparticles, J. Alloys Compd. 910 (2022), 164952.

[39] M.A. Islam, M. Zuba, V. DeBiase, N. Noviasky, C.J. Hawley, High capacity lithium ion batteries composed of cobalt oxide nanoparticle anodes and Raman spectroscopic analysis of nanoparticle strain dynamics in batteries, Nanotechnology 29 (2018), 075403.